Electronic and topological properties of Bi(110) ultrathin films grown on a Cu(111) substrate

Jufeng Wang, Xia Sun,[*] Hongjian Du, Chuanxu Ma, and Bing Wang[†]

*Hefei National Laboratory for Physical Sciences at the Microscale and Synergetic Innovation Center of Quantum Information
& Quantum Physics, Department of Physics, University of Science and Technology of China,
Hefei, Anhui 230026, People's Republic of China*

The electronic and topological properties of Bi(110) ultrathin films epitaxially grown on a Cu(111) substrate are investigated using scanning tunneling microscopy/spectroscopy, combined with density functional theory calculations. Bilayer-by-bilayer growth of the ultrathin Bi(110) films is observed, which manifests a structure of black-phosphorus-like Bi bilayers (BLs), with thickness up to 4 BLs. The surface atomic buckling heights in the 1-BL and 2-BL films are clearly identified to depend on the stacking modes with respect to the well-ordered Bi atoms in the adlayer covered on the Cu(111) surface. Our results demonstrate that while the electronic and topological properties of 1-BL films greatly depend on the stacking modes between the Bi(110) bilayer and the adlayer, the 2-BL films show well-decoupled electronic properties from the Cu substrate and nontrivial topologies robust against surface atomic buckling height benefitting from the interbilayer coupling. Our calculations further show that besides the parameter of buckling heights, the topological nontrivial-to-trivial transition can also be induced by changing the interbilayer distance and the vertical intralayer bond length.

I. INTRODUCTION

Two-dimensional (2D) topological insulators (TIs) [1] with spin-momentum-locked edge states protected from backscattering by time-reversal symmetry have attracted intensive interest due to promising applications in quantum spintronic devices [2,3]. As a heavy element, bismuth is an important element in many topological materials [4–9] because of its strong spin-orbit coupling [10]. The ultrathin Bi(111) (rhombohedral notation) film itself is proposed to be a 2D TI [11,12] but becomes topologically trivial when films are thicker than 8 bilayers (BLs) [13]. Alternatively, the growth of ultrathin Bi films in a few bilayers energetically prefers the (110) orientation with a black-phosphorus-like structure on many substrates, such as graphene [14], highly oriented pyrolytic graphite (HOPG) [15–18], Si(111) [19–21], Si(111)$\sqrt{3}\times\sqrt{3}$-B [22,23], black phosphorus (BP) [24], and transition metal dichalcogenides [25–27]. The electronic properties of films with a BP-like structure can be sensitively tuned by vertically stacking orders of layers [28–30] and strains either in plane or out of plane [31,32]. Recent reports show that the topological properties of 2D layers could also depend on stacking modes [33,34]. Moreover, BP-like Bi(110) ultrathin films can be an interesting platform to investigate novel electronic and topological properties, for instance, the theoretically predicted intriguing 2D Dirac and Weyl states [35].

Although ultrathin BP-like Bi(110) films have been studied on various substrates, the topological properties of these films are still controversial. For example, topologically trivial properties were suggested for 1-BL Bi(110) films grown on Si(111) [19] and black phosphorus [24], but topologically nontrivial properties were suggested for 1-BL and 2-BL Bi(110) films grown on HOPG [15]. It was also observed that the electronic topology could be tuned through strain engineering, the electric field, charge doping [15,32], and the film thickness [36,37]. These tuning effects on the variance in the electronic topology of Bi(110) films could be highly related to the atomic geometries, especially the buckling height h, i.e., the height difference between the two bonded Bi atoms in the topmost layer. For freestanding 1-BL and 2-BL Bi(110) films, a transition from topologically nontrivial to trivial was proposed at $h \sim 0.10$ Å and $h \sim 0.13$ Å, respectively [15]. However, the theoretically predicted h dependence of the electronic topology of ultrathin Bi bilayers and the tunability [15,32] still require experimental evidence.

In this paper, we investigate the dependence of the atomic buckling height in surfaces on the stacking modes for Bi(110) ultrathin films epitaxially grown on a Cu(111) substrate. We observe that BP-like Bi(110) islands, consisting of up to 4 bilayers, undergo a bilayer-by-bilayer growth mode on a well-ordered Bi adlayer on Cu(111). The stacking modes and the corresponding atomic geometries and the electronic properties in the surfaces are characterized using scanning tunneling microscopy/spectroscopy (STM/STS). In combination with first-principles calculations, we are able to connect the electronic topology to the surface atomic geometries that obviously depend on the stacking modes of BP-like Bi(110) bilayers. The dependence of the electronic topology on the interlayer and intralayer geometric parameters is also theoretically analyzed.

———————
*sunx@ustc.edu.cn
†bwang@ustc.edu.cn
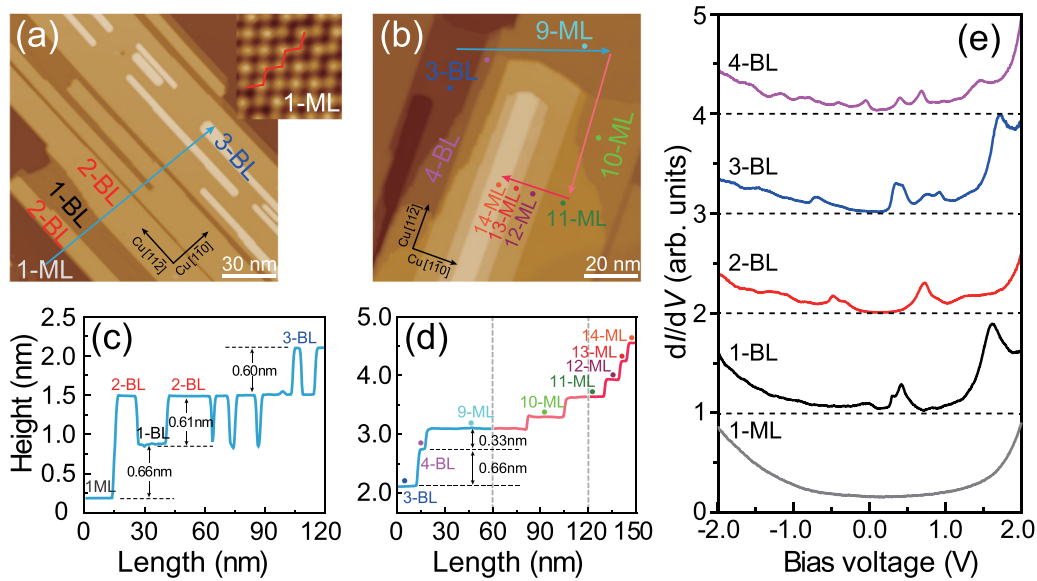
FIG. 1. (a) and (b) Large-scale STM images of Bi(110) islands grown on Cu(111) at nominal coverages of 1.19 and 3.32 nm. The images were taken at -1.0 V and 20 pA. The inset in (a) is an atomic-resolution image of the 1-ML adlayer, showing the Bi zigzag chains perpendicular to the ribbon edges. (c) and (d) Line profiles measured along the arrows in (a) and (b), respectively. Note that the labeled numbers of monolayers and bilayers of different thicknesses do not include the Bi adlayer. (e) Typical dI/dV spectra (set point current 1.0 nA at -2.0 V) recorded at the surfaces of the n-BL ($n = 1 - 4$) islands, with the dI/dV spectrum recorded at the 1-ML adlayer surface for comparison. The spectra are offset vertically for clarity, with the horizontal dashed lines indicating zero conductance.

II. EXPERIMENTAL AND THEORETICAL DETAILS

All STM experiments were performed in an ultrahigh-vacuum low-temperature STM (UNISOKU) with a base pressure better than 5×10^{-11} Torr, where a preparation chamber was equipped. The Cu(111) substrate was cleaned by several cycles of Ar$^+$ sputtering (20 min, 1000 eV) and annealing at 800 K for 30 min. The cleanness of the substrate was checked by STM images and STS spectra. Bi was deposited using a Knudsen cell at a deposition rate of 0.1 monolayer (ML)/min, and the film thickness was controlled by deposition time, which gave the nominal thickness of the prepared thin film. During the Bi evaporation, the substrate was kept at about 200 K. After the evaporation, the sample was transferred to the STM chamber without breaking the vacuum. All STM/STS measurements were carried out at 4.3 K with an electrochemically etched and well-cleaned tungsten tip. The dI/dV spectra were measured using a lock-in amplifier performed with a sinusoidal modulation of 5.0 mV (rms) at 791 Hz. The feedback loop of STM was turned off while acquiring the dI/dV spectra. The sample bias with respect to the tip was used.

Our calculations were mainly performed within the framework of density functional theory (DFT) using a plane-wave basis set, as implemented in the Vienna *Ab initio* Simulation Package (VASP) [38]. Electron exchange correlation interactions were described by the generalized gradient approximation (GGA) in the Perdew-Burke-Ernzerhof form [39]. The projector augmented-wave method was used to represent electron-ion interactions [40,41]. The Brillouin-zone integration was sampled with a Γ-centered $9 \times 11 \times 1$ k-point mesh. The van der Waals (vdW) corrections were included in calculations through the semiempirical dispersion correction

for density functionals (DFT-D3) [42]. The plane-wave energy cutoff was set to 500 eV. The films were calculated using a slab model including the BP-like Bi bilayer(s) on 1-ML Bi-covered three-layer Cu(111). A vacuum layer with a thickness larger than 17 Å was used to separate the slab. All Bi atoms and the Cu atoms in the topmost layer of the substrate were allowed to relax freely until the force on each atom was less than 0.01 eV/Å, and the Cu atoms in the bottom two layers were fixed. The spin-orbit coupling (SOC) was included in the calculations for the band structures and the density of states (DOS). The electronic structures were also calculated using the Heyd-Scuseria-Ernzerhof hybrid functional (HSE06) [43,44], which gives consistent results in comparison with results using GGA, except for the slightly enlarged band gap. The STM images were simulated using the Tersoff-Hamann approximation [45]. The topological invariant Z_2 was calculated following the method proposed by Soluyanov and Vanderbilt [46,47].

III. RESULTS AND DISCUSSION

Figures 1(a) and 1(b) show representative large-scale STM images for Bi(110) ultrathin films with different coverages grown on the Cu(111) substrate, where the Bi(110) islands tend to form a ribbonlike structure. The inset in Fig. 1(a) shows an atomic-resolution image of the Bi "wetting" layer, in which the Bi atoms locate alternately at the fcc and hcp hollow sites, forming zigzag chains along the $[1\bar{1}0]$ direction of the Cu(111) substrate and perpendicular to the bilayer ribbons [48,49]. Since the so-called wetting layer has a determined structure and coverage (slightly higher than half the atom number in each Bi bilayer or half the number
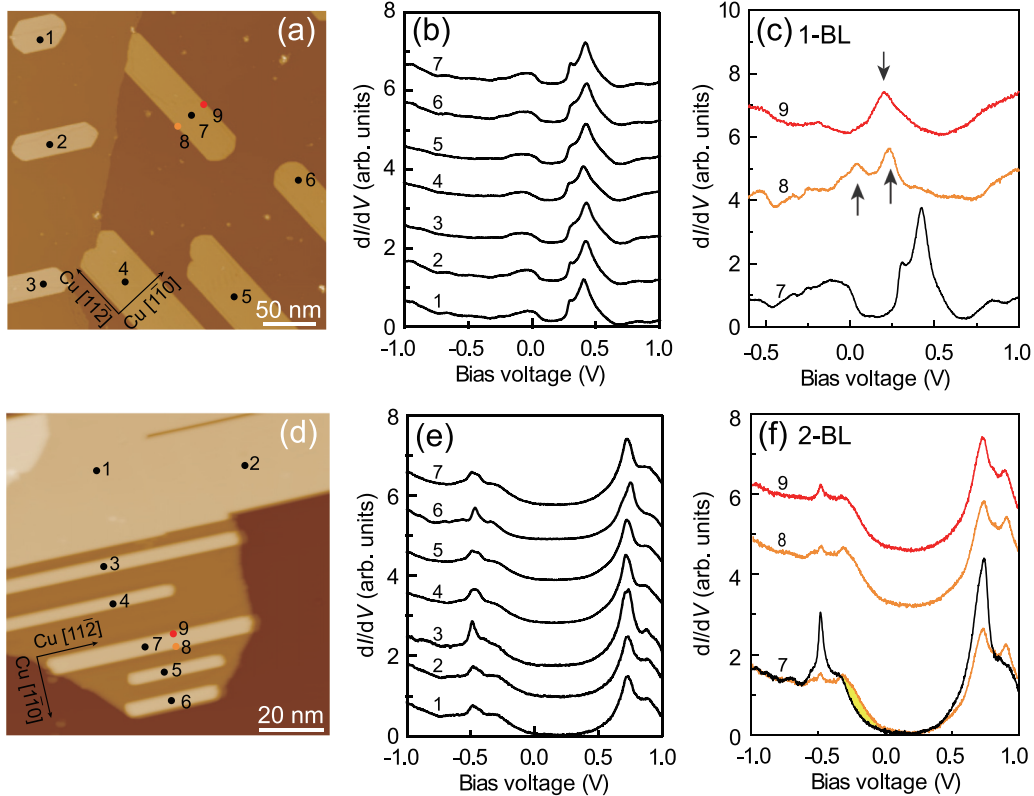
FIG. 2. (a) Large-scale STM image (-1.0 V and 200 pA) of the 1-BL Bi(110) islands. (b) dI/dV spectra (set point current 1.0 nA at -1.0 V) taken at the sites marked 1–7 in (a). (c) Typical dI/dV spectra (set point current 1.0 nA at -1.0 V) taken at the marked sites at the edges of the 1-BL Bi(110) island in (a), in comparison with that from the surface away from the edges. (d) Large-scale STM image (-1.0 V and 200 pA) of the 2-BL Bi(110) islands. (e) dI/dV spectra (set point current 1.0 nA at -1.0 V) taken at the sites marked 1–7 in (d). (f) Typical dI/dV spectra (set point current 1.0 nA at -1.0 V) taken at the marked sites at the edges of the 2-BL Bi(110) island in (d), in comparison with that from the surface away from the edges.

of Cu(111) surface lattice sites [49]), we prefer using "1-ML adlayer" instead of "wetting" layer. The existence of a Bi adlayer between the Bi(110) bilayer and the substrate was suggested before [15,16,18,50], but the structure of the adlayer was not resolved. In the measured line profiles [Figs. 1(c) and 1(d)], a typical height difference of about 0.60–0.66 nm between different ribbons is seen in the relatively thin film with a nominal thickness of 1.19 nm [Fig. 1(c)], but a height difference of about 0.33 nm becomes more dominant with island thickness higher than 2.7 nm [Fig. 1(d)]. The height difference of 0.66 nm for the ribbons is in agreement with the height of Bi bilayers with BP-like structure that were observed on different substrates [18–20,22,36]. Hence, the ribbons observed in thinner Bi films can be assigned to Bi bilayers with BP-like structure. According to the heights with respect to the 1-ML adlayer, we label the BP-like ribbons as n-BL ($n = 1, 2, 3, \ldots$), and up to 4-BL ribbons or terraces are observed. The higher layers thereafter change to have a layer-by-layer growth mode, indicating the films more likely changing to a bulk structure of Bi(110) rather than the BP-like structure in the thicker layers.

Figure 1(e) shows the typical dI/dV spectra recorded at different Bi bilayers. The dI/dV spectrum recorded at the 1-ML Bi adlayer is also shown for comparison, in which the U-shaped spectrum with metallic states was characterized in our previous work [48]. The spectrum recorded at 1-BL

islands shows a gaplike feature above the Fermi level E_F, but the spectrum still shows its metallic characteristics, indicating that the 1-ML Bi adlayer does not sufficiently decouple the 1-BL islands from the Cu substrate. Interestingly, the spectrum recorded at 2-BL islands shows an energy gap around E_F, which is quite similar to the semiconducting features observed in the 1-BL Bi(110) islands grown on HOPG [15] and in the 2-BL Bi(110) ribbons grown on graphene [14]. Note that such a semiconducting behavior has been theoretically predicted for freestanding 1-BL Bi(110) films [15,36]. This observation means that in the 2-BL islands the bottom Bi bilayer acts as a good decoupling layer for the top Bi bilayer, making the 2-BL islands behave like a semiconductor [51]. The spectra recorded at 3-BL and 4-BL islands again show metallic characteristics, which reflect a semiconductor-semimetal transition occurring at about 3-BL and 4-BL islands because of the enhanced interlayer coupling in the thicker films. For films thicker than 4 BLs, they thereafter change to layer-by-layer growth, showing metallic features more and more similar to the Bi(110) bulk phase with the increase of the film thickness [51]. In the following discussion, we focus on the geometries and electronic properties of the 1-BL and 2-BL films.

Although the widths and lengths of the 1-BL and 2-BL islands have relatively wide distributions ranging from about 2 nm to several tens of nanometers [Figs. 2(a) and 2(d)], the main features in the dI/dV spectra do not obviously

depend on the widths or lengths [Figs. 2(b) and 2(e)]. Such independence of the island sizes suggests that the bulk electronic structures of the 1-BL and 2-BL island surfaces are not obviously affected by the island size. At the edges of the 1-BL and 2-BL islands, the typical dI/dV spectra [orange and red curves in Figs. 2(c) and 2(f)] were measured and are different from those of the surfaces. The different features at the edges may be related to the topological electronic properties. It is noticed that, as marked by the black arrows in Fig. 2(c), the dI/dV spectra on different sides of the edges in the 1-BL islands commonly show quite different electronic states, which may be due to the asymmetric configurations at the edge terminals. Differently, the dI/dV spectra on both sides of the edges in the 2-BL islands show quite similar features [Fig. 2(f)], indicating their nearly identical atomic configurations at both terminals and thus nearly identical electronic states. In a comparison of the dI/dV spectra between the edge and the surface, additional electronic states can be observed in 2-BL islands, as marked by the shading in Fig. 2(f), which may be a hint for the edge states. However, the different atomic structures at the edge terminals between the 1-BL and 2-BL islands [51] could be another factor inducing a difference in the electronic states. Whether these features are related to the topological electronic properties or not demands further investigation, which could be a topic of focus in another work.

We further use the atomic-resolution STM images to characterize the actual stacking modes and buckling heights. As shown in Fig. 3, the stacking modes can be resolved in the atomic-resolution images for the 1-BL and 2-BL islands with respect to the Bi atoms in the 1-ML adlayer and in the first BP-like bilayer, respectively. It is observed that the stacking mode between the first and second BLs is dominantly AA stacking, in which the Bi atoms in the second bilayer are on the top site of the Bi atoms in the first bilayer [Figs. 3(c) and 3(f)]. However, for the Bi atoms in the 1-BL island relative to the Bi atoms in the 1-ML adlayer, there are two types of stacking modes; that is, the Bi atoms in the 1-BL island locate over either the hollow sites [Fig. 3(b)] or the top sites [Fig. 3(e)] of the Bi atoms in the 1-ML adlayer on Cu(111), as marked by the superposed structural models. The different stacking modes lead to different contrasts of the corner and central atoms of the unit cells, reflecting quite different atomic geometries as a result of different buckling heights in the topmost layers [51].

The experimentally observed different stacking modes are schematically illustrated in Fig. 4(a). The main difference of the two models is the locations of the Bi atoms in the 1-BL layer over either the hollow sites or the top sites of the 1-ML Bi adlayer on Cu(111), denoted as hollow-site and top-site models, respectively. For the 2-BL film, an AA stacking mode between the first and second BP-like bilayers is adopted according to our observations. Our calculations further confirm that the AA stacking has the lowest energy among four possible stacking modes [51]. Surface lattice constants of $a = 5.00$ Å and $b = 4.54$ Å, perpendicular to and along the zigzag chain direction, respectively, are adopted according to the values measured in the STM images. The elongated lattice constant ($a = 5.00$ Å) indicates that an in-plane tensile strain (5.2%) is introduced in the Bi films in the direction along **a**, in comparison with the lattice constant of 4.75 Å
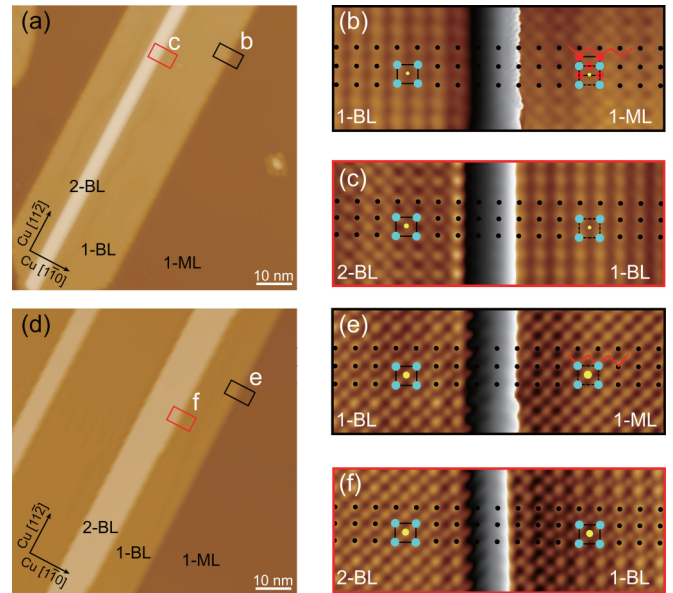
FIG. 3. (a) Large-scale STM image (-1.0 V and 50 pA). (b) and (c) High-contrast atomic-resolution images (-50 mV and 1.0 nA) of the rectangles marked b and c in (a). (d) Large-scale image (-1.0 V and 50 pA). (e) and (f) High-contrast atomic-resolution images (-50 mV and 1.0 nA) of the rectangles marked e and f in (d). The black dots represent the lattice of the higher island with extension to the lower island. A half-unit-cell shift between the lattices of the 1-BL island and the 1-ML adlayer in (b) indicates the 1-BL island is located over the hollow sites of the 1-ML adlayer. The lattices overlapping in (e) suggest the 1-BL island is located over the top sites of the 1-ML adlayer. For the 2-BL islands, the lattices are overlapped for the higher and lower bilayers in (c) and (f), as indicated by the unit cells with colored dots, showing an AA stacking mode. The buckling height of the central atom is schematically indicated by the dot size in yellow according to their visibility in the images.

in bulk crystal [52]. Such a stretch was also theoretically proposed to be the favorite for its nontrivial topological phase [32]. While for the stacking between the 1-BL film and the 1-ML adlayer the top-site model has a slightly lower energy than the hollow-site model without the inclusion of the vdW interaction, inversely, the hollow-site model has a much lower energy than the top-site model with the inclusion of the vdW interaction in our calculations (Table I). Our statistic ratios of 1-BL Bi(110) with hollow-site and top-site stacking modes are 91.3% and 8.7% [51], respectively, which qualitatively agree with the calculated energy difference with the vdW correction. It should be noted that for the 2-BL island the energy difference ($\sim$66 meV) between the two models is relatively small where the coexistence of both stacking modes can be expected. Our calculations also show that the buckling heights are $h = 0.225$ and 0.009 Å for the 1-BL films and $h = 0.209$ and 0.006 Å for the 2-BL films using the hollow-site and top-site models (Table I), respectively. The simulated images well reproduce the features experimentally observed in the STM images of the 1-BL and 2-BL islands [Figs. 4(b) and 4(c)]. The most distinct difference in these features is the relative contrast of the central Bi atom within a unit cell in the topmost surface layer. It is seen that the central Bi
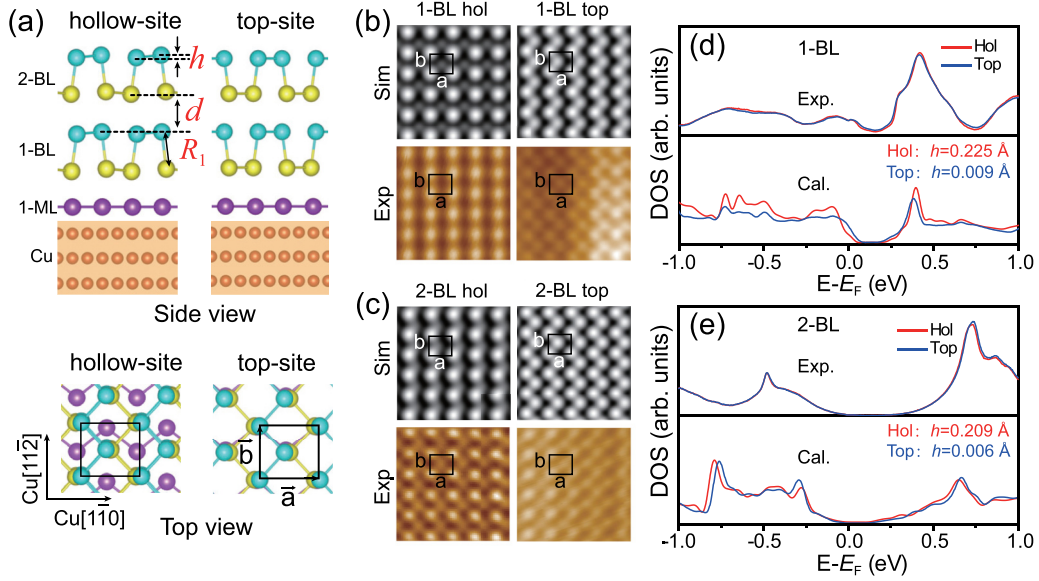
FIG. 4. (a) Structural models of the 2-BL Bi(110) island with AA stacking between the first and second BLs in the side view and top view. The Bi atoms in the BP-like bilayers locate over the hollow site (left) and the top site (right) with respect to the Bi atoms in the 1-ML adlayer (zigzagged chains along the Cu[1$\bar{1}$0] direction). For the 1-BL Bi(110) island, similar structural models are used by removing the second bilayer. h defines the buckling height in the topmost Bi layer, d defines the interlayer distance, and R_1 defines the vertically oriented intralayer bond length in the first bilayer. In the unit cell (black rectangle) $a = 5.00$ Å and $b = 4.54$ Å. (b) and (c) Comparison of the simulated (top panel) and experimental (bottom panel) results for the 1-BL and 2-BL islands, respectively. The STM images were recorded in the constant-current mode at −100 mV and 1.0 nA. The simulated images were obtained by integrating the states from the Fermi level to −0.1 eV at a tip height of 4 Å above the topmost atomic layer, with the isosurface of 1.2×10^{-6} e/Å^3. Image size is 2.5×2.5 nm^2. (d) and (e) Comparison of the dI/dV spectra (set point current of 1.0 nA at −1.0 V.) and the DFT-calculated partial DOSs contributed by the p_z orbital for 1-BL and 2-BL Bi(110) films, respectively. A Gaussian broadening of 15 meV is used for the calculated DOSs.

atom is not very pronounced in the simulated images using the hollow-site model, in line with the very large calculated buckling height. In contrast, for the top-site model, the central Bi atom becomes obviously visible and even has a contrast comparable to the corner atoms, leading to the observation of zigzaglike chains. Taking into consideration our experimental and theoretical results, we believe that the existence of electronic topology is more promising in 2-BL islands.

Figures 4(d) and 4(e) show that the main features of the experimental dI/dV spectra are highly comparable to those of the calculated DOSs of the 1-BL and 2-BL structures, respectively. Note that the calculated DOSs are from the 1-BL and 2-BL structures isolated after the removal of the substrate [1-ML Bi-covered Cu(111)], where the geometric parameters

TABLE I. Calculated energy difference (per unit cell) between the hollow-site and the top-site models and buckling height h in the topmost Bi layer of 1-BL and 2-BL films. $\Delta E = E_h - E_t$, where E_h (h_h) and E_t (h_t) are the energies (bucking heights) obtained using the hollow-site and top-site models, respectively, and ΔE^v is obtained with the inclusion of vdW interactions in the calculations.

	1-BL film	2-BL film
ΔE (meV)	+6.01	+51.13
ΔE^v (meV)	−110.49	−66.04
h_h (Å)	0.225	0.209
h_t (Å)	0.009	0.006

are the same as those in optimized structures with the substrate and considering different stacking modes between the first bilayer and the 1-ML Bi adlayer [51]. Such a treatment neglects the contributions of the metallic states of the Cu substrate to the DOSs of the 1-BL and 2-BL film surfaces, which mainly lead to the gaplike feature in the calculated DOSs that is different from the metallic feature in the experimental spectra in the 1-BL film [Fig. 4(d)]. Nevertheless, while different stacking orders between the bilayers may significantly affect the electronic properties of BP-like structures [29,30], our calculations confirm that only the experimentally observed AA stacking well reproduces the STS results [51]. Interestingly, it is seen that the difference between the experimental and calculated results is almost negligible in the 2-BL film [Fig. 4(e)], which means that the first bilayer in the 2-BL film acts as a good decoupling layer.

Figures 5(a) and 5(b) give the band structures of the isolated 1-BL and 2-BL Bi(110) films with optimized geometric parameters using the hollow-site (red lines) and top-site (blue lines) models, respectively, where the band structures are calculated by removing the 1-ML adlayer and Cu substrate. The main characteristics of the band structures calculated with different stacking modes are quite similar for the 1-BL and 2-BL Bi(110) films. The calculated band gaps are about 154 and 121 meV for the 1-BL films and 64 and 73 meV for the 2-BL films in the hollow-site and top-site models, respectively. Similar band structures are also obtained using HSE functionals with slightly enlarged band gap values [51]. Due
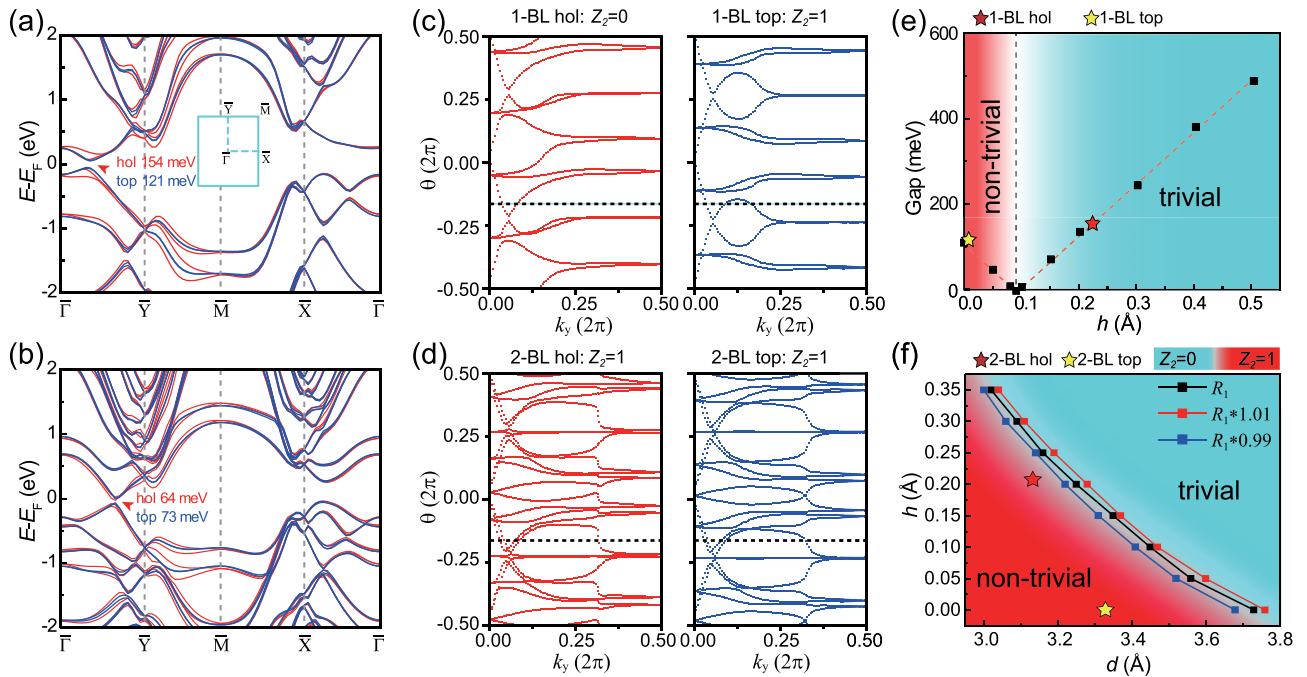
FIG. 5. (a) and (b) Band structures of isolated 1-BL and 2-BL BP-like Bi(110) films with the atomic geometries using the hollow-site (red lines) and top-site (blue lines) models by removing the 1-ML adlayer and Cu substrate. The inset in (a) shows the Brillouin zone. (c) and (d) Evolutions of Wannier charge centers along k_y for the isolated 1-BL and 2-BL Bi(110) films, using the hollow-site (left panels) and the top-site (right panels) models, respectively. (e) h dependence of the band gap and the topological phase of 1-BL Bi(110) films. The red and yellow stars are results corresponding to 1-BL Bi(110) using the hollow-site and top-site models, respectively. (f) Topological phase diagram of 2-BL Bi(110) films as a function of atomic buckling h, the interlayer distance d, and the vertically oriented intralayer bond length R_1. The basic structure adopted in (f) is the isolated 2-BL films with optimized geometries using the hollow-site model, and the values of h, d, and R_1 are adjusted manually.

to the relatively small gaps and the influence of the substrate, the gaps may not be resolved in the dI/dV spectra [Figs. 4(d) and 4(e)].

Nevertheless, we may analyze the topological properties of Bi(110) films by calculating the Z_2 invariant using a tight-binding model. Figures 5(c) and 5(d) show the evolution of the Wannier charge center (WCC), calculated with the method proposed by Soluyanov and Vanderbilt [46,47], for the isolated 1-BL and 2-BL Bi(110) films using the optimized hollow-site and top-site geometries. The Z_2 topological invariant can be determined by the number of crossings between any arbitrary horizontal reference line and the evolution of the WCC along k_y or k_x. The even and odd crossings correspond to the topologically trivial and nontrivial phases, respectively. The horizontal reference line indicates an even number of crossings [left panel of Fig. 5(c)], suggesting that the 1-BL Bi(110) with the hollow-site geometry is topologically trivial ($Z_2 = 0$). However, the number of crossings [right panel of Fig. 5(c)] is odd, demonstrating that the 1-BL Bi(110) with the top-site geometry is topologically nontrivial ($Z_2 = 1$). Figure 5(e) shows the dependence of the band gap and the topological properties on the atomic buckling height h for the 1-BL Bi(110) film with an elongated lattice parameter ($a = 5.00$ Å). Similar to the results reported by Lu *et al.* [15], the band gap varies linearly with the deviation of h from 0.10 Å, and a topological trivial-nontrivial phase transition occurs at $h_c = 0.10$ Å [51]. In agreement with the previous report, the topological properties of 1-BL Bi(110) can be tuned

by the atomic buckling h, which may be achieved by different stacking modes between the 1-BL films and the 1-ML adlayer [Figs. 5(c) and 5(e)].

It is interesting to observe that the topological invariant is independent of the stacking modes for the 2-BL Bi(110) films, remaining $Z_2 = 1$ for both the hollow-site and top-site geometries [Fig. 5(d)]. The atomic buckling of the 2-BL films stacked over the hollow site is as large as 0.209 Å, considerably larger than the critical value of $h_c \sim 0.1$ Å for 1-BL Bi(110), exhibiting a higher tolerance for atomic buckling than the 1-BL films. It is worth noting that, except for the atomic buckling, there are obvious differences in the interlayer distance d (3.15/3.33 Å) and the vertical intralayer bond length R_1 (3.10/3.15 Å) for the optimized structures of the 2-BL Bi(110) islands stacked over the hollow site and the top site. Therefore, we have calculated Z_2 as a function of the atomic buckling h, the interlayer distance d, and the vertical intralayer bond length R_1. The results are shown in Fig. 5(f). The hollow-site geometry is used as a basic structure, and we manually change the values of h, d, or R_1 in each calculation. Similar to that of 1-BL Bi(110), the increase of the atomic buckling induces a topologically nontrivial [$Z_2 = 1$, Fig. 5(f), in red] to trivial [$Z_2 = 0$, Fig. 5(f), in cyan] transition when d and R_1 are fixed. On the other hand, Z_2 can also be changed from 1 to 0 by the enlargement of the interlayer distance when h and R_1 are fixed. The interlayer distance of the hollow-site geometry is less than that of the top-site one by about 0.18 Å. The smaller d is a favorable condition for 2-BL Bi(110) to

maintain the topologically nontrivial states that thus have a higher tolerance for the atomic buckling. The third important factor for the topological properties is the vertical intralayer bond length R_1. Compared with its value for freestanding 2-BL Bi(110), R_1 is elongated by about 1% due to the influence of the 1-ML adlayer and the Cu substrate. The black squares in Fig. 5(f) are calculated with R_1 equal to that of the hollow-site structure. The red and blue squares are computed with R_1 elongated and shortened by 1%, respectively. It is clear that the elongation of R_1 expands the area of the nontrivial topology, which is also helpful for enhancing the tolerance for atomic buckling. Consequently, the 2-BL Bi(110) islands are topologically nontrivial even when stacked over the hollow site (with h as large as 0.209 Å), showing a robust nontrivial topological behavior.

IV. CONCLUSIONS

In summary, the structural, electronic, and topological properties of BP-like Bi(110) ultrathin films on Cu(111) were investigated by STM/STS measurements and DFT calculations. The well-ordered Bi adlayer on Cu(111) acts as a template for the bilayer-by-bilayer growth of BP-like Bi(110) islands up to 4 bilayers, which is thereafter followed by layer-by-layer growth to form the Bi(110) bulk phase. The atomic-resolution STM images enable us to determine the stacking modes. A transition from semiconductor to semimetal is revealed by an increase in the film thickness. For 1-BL Bi(110) films, the topological properties can be tuned by stacking modes between the Bi(110) BLs and the Bi adlayer, which induces a large difference in the atomic buckling. For 2-BL Bi(110) films, the topological properties are independent of the stacking modes, showing a robust nontrivial topology, enhanced by interlayer coupling. The topologically nontrivial ($Z_2 = 1$) to trivial ($Z_2 = 0$) transition can be induced not only by increasing the atomic buckling but also by elongating the inter-bilayer distance and shortening the vertical intralayer bond length. Our studies provide insights into the tunable electronic and topological properties of BP-like Bi(110) films.

[1] A. Bansil, H. Lin, and T. Das, Colloquium: Topological band theory, Rev. Mod. Phys. **88**, 021004 (2016).

[2] D. Awschalom and N. Samarth, Spintronics without magnetism, Physics **2**, 50 (2009).

[3] A. Manchon, H. C. Koo, J. Nitta, S. M. Frolov, and R. A. Duine, New perspectives for Rashba spin-orbit coupling, Nat. Mater. **14**, 871 (2015).

[4] Y. L. Chen, J. G. Analytis, J. H. Chu, Z. K. Liu, S. K. Mo, X. L. Qi, H. J. Zhang, D. H. Lu, X. Dai, Z. Fang, S. C. Zhang, I. R. Fisher, Z. Hussain, and Z. X. Shen, Experimental realization of a three-dimensional topological insulator, Bi_2Te_3, Science **325**, 178 (2009).

[5] D. Hsieh, Y. Xia, D. Qian, L. Wray, J. H. Dil, F. Meier, J. Osterwalder, L. Patthey, J. G. Checkelsky, N. P. Ong, A. V. Fedorov, H. Lin, A. Bansil, D. Grauer, Y. S. Hor, R. J. Cava, and M. Z. Hasan, A tunable topological insulator in the spin helical Dirac transport regime, Nature (London) **460**, 1101 (2009).

[6] H. J. Zhang, C. X. Liu, X. L. Qi, X. Dai, Z. Fang, and S. C. Zhang, Topological insulators in Bi_2Se_3, Bi_2Te_3 and Sb_2Te_3 with a single Dirac cone on the surface, Nat. Phys. **5**, 438 (2009).

[7] Z. Wang, Y. Sun, X.-Q. Chen, C. Franchini, G. Xu, H. Weng, X. Dai, and Z. Fang, Dirac semimetal and topological phase transitions in A_3Bi (A = Na, K, Rb), Phys. Rev. B **85**, 195320 (2012).

[8] G. Autès, A. Isaeva, L. Moreschini, J. C. Johannsen, A. Pisoni, R. Mori, W. Zhang, T. G. Filatova, A. N. Kuznetsov, L. Forró, W. Van den Broek, Y. Kim, K. S. Kim, A. Lanzara, J. D. Denlinger, E. Rotenberg, A. Bostwick, M. Grioni, and O. V. Yazyev, A novel quasi-one-dimensional topological insulator in bismuth iodide β-Bi_4I_4, Nat. Mater. **15**, 154 (2016).

[9] C.-C. Liu, J.-J. Zhou, Y. Yao, and F. Zhang, Weak Topological Insulators and Composite Weyl Semimetals: β-Bi_4X_4 (X=Br, I), Phys. Rev. Lett. **116**, 066801 (2016).

[10] M. Bieniek, T. Woźniak, and P. Potasz, Study of spin-orbit coupling effect on bismuth (111) bilayer, Acta. Phys. Pol. A **130**, 609 (2016).

[11] S. Murakami, Quantum Spin Hall Effect and Enhanced Magnetic Response by Spin-Orbit Coupling, Phys. Rev. Lett. **97**, 236805 (2006).

[12] M. Wada, S. Murakami, F. Freimuth, and G. Bihlmayer, Localized edge states in two-dimensional topological insulators: Ultrathin Bi films, Phys. Rev. B **83**, 121310(R) (2011).

[13] H. W. Yeom, K.-H. Jin, and S.-H. Jhi, Topological fate of edge states of single Bi bilayer on Bi(111), Phys. Rev. B **93**, 075435 (2016).

[14] J.-T. Sun, H. Huang, S. L. Wong, H. J. Gao, Y. P. Feng, and A. T. S. Wee, Energy-Gap Opening in a Bi(110) Nanoribbon Induced by Edge Reconstruction, Phys. Rev. Lett. **109**, 246804 (2012).

[15] Y. Lu, W. Xu, M. Zeng, G. Yao, L. Shen, M. Yang, Z. Luo, F. Pan, K. Wu, T. Das, P. He, J. Jiang, J. Martin, Y. P. Feng, H. Lin, and X.-S. Wang, Topological properties determined by atomic buckling in self-assembled ultrathin Bi(110), Nano Lett. **15**, 80 (2015).

[16] P. J. Kowalczyk, O. Mahapatra, S. A. Brown, G. Bian, X. Wang, and T.-C. Chiang, Electronic size effects in three-dimensional nanostructures, Nano Lett. **13**, 43 (2013).

[17] P. J. Kowalczyk, O. Mahapatra, D. Belić, S. A. Brown, G. Bian, and T.-C. Chiang, Origin of the moiré pattern in thin Bi films deposited on HOPG, Phys. Rev. B **91**, 045434 (2015).

[18] P. J. Kowalczyk, O. Mahapatra, D. N. McCarthy, W. Kozlowski, Z. Klusek, and S. A. Brown, STM and XPS investigations of bismuth islands on HOPG, Surf. Sci. **605**, 659 (2011).

[19] T. Nagao, J. T. Sadowski, M. Saito, S. Yaginuma, Y. Fujikawa, T. Kogure, T. Ohno, Y. Hasegawa, S. Hasegawa, and T. Sakurai, Nanofilm Allotrope and Phase Transformation of Ultrathin Bi Film on Si(111)-7×7, Phys. Rev. Lett. **93**, 105501 (2004).

[20] S. Yaginuma, T. Nagao, J. T. Sadowski, M. Saito, K. Nagaoka, Y. Fujikawa, T. Sakurai, and T. Nakayama, Origin of flat morphology and high crystallinity of ultrathin bismuth films, Surf. Sci. **601**, 3593 (2007).

[21] S. Yaginuma, T. Nagao, G. Bihlmayer, Y. Koroteev, E. Chulkov, and T. Nakayama, Electronic structure of ultrathin bismuth films with A7 and black-phosphorus-like structures, J. Phys. Soc. Jpn. **77**, 014701 (2007).

[22] K. Nagase, I. Kokubo, S. Yamazaki, K. Nakatsuji, and H. Hirayama, Structure and growth of Bi(110) islands on Si(111)$\sqrt{3}\times\sqrt{3}$-B substrates, Phys. Rev. B **97**, 195418 (2018).

[23] K. Nagase, R. Ushioda, K. Nakatsuji, T. Shirasawa, and H. Hirayama, Growth of extremely flat Bi(110) films on a Si(111)$\sqrt{3}\times\sqrt{3}$-B substrate, Appl. Phys. Express **13**, 085506 (2020).

[24] S. Ju, M. Wu, H. Yang, N. Wang, Y. Zhang, P. Wu, P. Wang, B. Zhang, K. Mu, Y. Li, D. Guan, D. Qian, F. Lu, D. Liu, W.-H. Wang, X. Chen, and Z. Sun, Band structures of ultrathin Bi(110) films on black phosphorus substrates using angle-resolved photoemission spectroscopy, Chin. Phys. Lett. **35**, 077102 (2018).

[25] X. Dong, Y. Li, J. Li, X. Peng, L. Qiao, D. Chen, H. Yang, X. Xiong, Q. Wang, X. Li, J. Duan, J. Han, and W. Xiao, Epitaxial growth and structural properties of Bi(110) thin films on TiSe$_2$ substrates, J. Phys. Chem. C **123**, 13637 (2019).

[26] L. Peng, J. Qiao, J.-J. Xian, Y. Pan, W. Ji, W. Zhang, and Y.-S. Fu, Unusual electronic states and superconducting proximity effect of Bi films modulated by a NbSe$_2$ substrate, ACS Nano **13**, 1885 (2019).

[27] J.-Y. Liu, H.-H. Sun, D.-D. Guan, Y.-Y. Li, S.-Y. Wang, C.-H. Liu, H. Zheng, and J.-F. Jia, Scanning tunneling microscopy research of Bi(110) thin films grown on NbSe$_2$, Acta Phys. Sin. **67**, 170701 (2018).

[28] J. Dai and X. C. Zeng, Bilayer phosphorene: Effect of stacking order on bandgap and its potential applications in thin-film solar cells, J. Phys. Chem. Lett. **5**, 1289 (2014).

[29] H. Shu, Y. Li, X. Niu, and J. Wang, The stacking dependent electronic structure and optical properties of bilayer black phosphorus, Phys. Chem. Chem. Phys. **18**, 6085 (2016).

[30] C. Xia, J. Du, W. Xiong, Y. Jia, Z. Wei, and J. Li, A type-II GeSe/SnS heterobilayer with a suitable direct gap, superior optical absorption and broad spectrum for photovoltaic applications, J. Mater. Chem. A. **5**, 13400 (2017).

[31] G. Moynihan, S. Sanvito, and D. O'Regan, Strain-induced Weyl and Dirac states and direct-indirect gap transitions in group-V materials, 2D Mater. **4**, 045018 (2017).

[32] S.-S. Li, W.-X. Ji, P. Li, S.-J. Hu, L. Cai, C.-W. Zhang, and S.-S. Yan, Tunability of the quantum spin hall effect in Bi(110) films: Effects of electric field and strain engineering, ACS Appl. Mater. Interfaces **9**, 21515 (2017).

[33] R. Peng, Y. Ma, H. Wang, B. Huang, and Y. Dai, Stacking-dependent topological phase in bilayer MBi$_2$Te$_4$ (M = Ge, Sn, Pb), Phys. Rev. B **101**, 115427 (2020).

[34] L. Kou, C. Niu, H. Fu, Y. Ma, B. Yan, and C. Chen, Tunable quantum order in bilayer Bi$_2$Te$_3$: Stacking dependent quantum spin Hall states, Appl. Phys. Lett. **112**, 243103 (2018).

[35] K.-H. Jin, H. Huang, Z. Wang, and F. Liu, A 2D nonsymmorphic Dirac semimetal in a chemically modified group-VA monolayer with a black phosphorene structure, Nanoscale **11**, 7256 (2019).

[36] G. Bian, X. Wang, T. Miller, T. C. Chiang, P. J. Kowalczyk, O. Mahapatra, and S. A. Brown, First-principles and spectroscopic studies of Bi(110) films: Thickness-dependent Dirac modes and property oscillations, Phys. Rev. B **90**, 195409 (2014).

[37] E. Aktürk, O. Ü. Aktürk, and S. Ciraci, Single and bilayer bismuthene: Stability at high temperature and mechanical and electronic properties, Phys. Rev. B **94**, 014115 (2016).

[38] G. Kresse and J. Furthmüller, Efficient iterative schemes for *ab initio* total-energy calculations using a plane-wave basis set, Phys. Rev. B **54**, 11169 (1996).

[39] J. P. Perdew, K. Burke, and M. Ernzerhof, Generalized Gradient Approximation Made Simple, Phys. Rev. Lett. **77**, 3865 (1996).

[40] G. Kresse and D. Joubert, From ultrasoft pseudopotentials to the projector augmented-wave method, Phys. Rev. B **59**, 1758 (1999).

[41] P. E. Blöchl, Projector augmented-wave method, Phys. Rev. B **50**, 17953 (1994).

[42] S. Grimme, J. Antony, S. Ehrlich, and H. Krieg, A consistent and accurate *ab initio* parametrization of density functional dispersion correction (DFT-D) for the 94 elements H-Pu, J. Chem. Phys. **132**, 154104 (2010).

[43] J. Heyd, G. E. Scuseria, and M. Ernzerhof, Hybrid functionals based on a screened Coulomb potential, J. Chem. Phys. **118**, 8207 (2003).

[44] J. Heyd, G. E. Scuseria, and M. Ernzerhof, Erratum: "Hybrid functionals based on a screened Coulomb potential" [J. Chem. Phys. **118**, 8207 (2003)], J. Chem. Phys. **124**, 219906 (2006).

[45] J. Tersoff and D. R. Hamann, Theory of the scanning tunneling microscope, Phys. Rev. B **31**, 805 (1985).

[46] A. A. Soluyanov and D. Vanderbilt, Wannier representation of Z$_2$ topological insulators, Phys. Rev. B **83**, 035108 (2011).

[47] A. A. Soluyanov and D. Vanderbilt, Computing topological invariants without inversion symmetry, Phys. Rev. B **83**, 235401 (2011).

[48] M. Tian, J. Wang, X. Liu, W. Chen, Z. Liu, H. Du, X. Ma, X. Cui, A. Zhao, Q. Shi, Z. Wang, Y. Luo, J. Yang, B. Wang, and J. G. Hou, Creation of the Dirac nodal line by extrinsic symmetry engineering, Nano Lett. **20**, 2157 (2020).

[49] D. Kaminski, P. Poodt, E. Aret, N. Radenovic, and E. Vlieg, Surface alloys, overlayer and incommensurate structures of Bi on Cu(111), Surf. Sci. **575**, 233 (2005).

[50] X. Wang, X. Yang, N. Shen, B. Wang, G. Ge, G. Wang, and J. Wan, Atomistic insights into the growth of Bi (110) thin films on Cu (111) substrate, Appl. Surf. Sci. **481**, 1449 (2019).

[51] See Supplemental Material at http://link.aps.org/supplemental/10.1103/PhysRevB.105.115407 for additional details about STS data for films thicker than 2 BLs, stacking modes of 1-BL and 2-BL films, electronic structures of 1-BL and 2-BL films with and without a substrate, band structures of films with thicknesses from 1 to 4 BLs, and the variation of band structures with atomic buckling of 1-BL and 2-BL films.

[52] P. Hofmann, The surfaces of bismuth: Structural and electronic properties, Prog. Surf. Sci. **81**, 191 (2006).